MECHANICS OF COHESIVE-FRICTIONAL MATERIALS, VOL. 2, 279–299 (1997)

Hypoplastic model for cohesionless soils with elastic strain range

A. Niemunis[1]* and I. Herle[2]*

[1] *Technical University of Gdańsk, Poland*
[2] *Czech Academy of Sciences, Czech Republic*

SUMMARY

In order to eliminate ratcheting a so-called intergranular strain has been added to a hypoplastic constitutive model. This additional state variable represents the deformation of the interface layer between the grains. The new concept is outlined and comparisons with and without intergranular strain are presented. Some comments on numerical implementation and determination of material constants are made. A discussion on the uniqueness of the solution and objectivity of the rate of intergranular strain is added. © 1997 John Wiley & Sons, Ltd.

Mech. of Cohes.-Frict. Mater., **2**, 279–299 (1997)

No. of Figures: 21. No. of Tables: 1. No. of References: 41.

KEY WORDS: constitutive model; hypoplasticity; plasticity; grain contacts; intergranular strain; strain-space plasticity; recent history; small strain; ratcheting

1. INTRODUCTION

The theory of hypoplasticity has been developed by Kolymbas and Gudehus and their associates since the late seventies.[1–8] Similar models have also been proposed independently by other authors, e.g., Reference 9. Hypoplastic models have been shown to perform very well for deformations due to rearrangements of the grain skeleton. However, application of hypoplasticity to cyclic stressing or deformation with small amplitudes (e.g., Reference 10) reveals some defects. The most striking shortcoming is an excessive accumulation of deformation predicted for small stress cycles, called ratcheting. For undrained cyclic shearing the hypoplastic approach predicts too large a build-up of pore pressure.[3] Neither the small-strain stiffness nor effects of the recent history have been adequately modelled by hypoplasticity as yet.

The purpose of the present paper is to extend hypoplasticity to improve the small strain performance after changes of direction of stress or strain path. We assume that the material is dry or fully saturated and that thermal, chemical and electrical effects can be disregarded. We also neglect viscosity.

The behaviour of granular soils is incrementally non-linear even at low strains except for a small elastic range, not exceeding ca. 10^{-5}.[11] In this range the stiffness is higher and approximately independent of strains. Values can be obtained with precise measuring of displacements (LVDT, proximity transducers). Alternatively, they can be calculated from *P*-wave or *S*-wave velocities (resonant column, bender elements). The size of the elastic range in strain space is reported rather to

* Current address: Institut für Bodenmechanik und Felsmechanik, Universität Karlsruhe, Postfach 6980, 76128 Karlsruhe, Germany.

CCC 1082–5010/97/040279–21 $17.50

Received 5 March 1996
Revised 10 October 1996

be independent of stress and void ratio, and the elastic stiffness depends on stress and density in a similar manner to the incremental stiffness during monotonic deformation.[12]

Depending on the deformation history, the stiffness, at a given stress and density and for a certain direction of strain rate, can have different values. In particular, for any sharp change of direction of the strain path an increase of stiffness is observed, and the maximum value appears with a complete (i.e., 180°) strain rate reversal.[13] If straining is continued with nearly the same direction the stiffness decreases gradually, and after a certain strain path, of length called $\varepsilon_{\mathrm{SOM}}$ (measured from the reversal), the stiffness regains the low value typical for a monotonic path (SOM is an abbreviation for *swept-out memory*).[14]

Micromechanical considerations[15–17] indicate that intergrangular forces are transferred through thin amorphous zones in the intergranular interface. We propose a concept of an elastic range that is qualitatively related with properties of such zones. We formulate the elastic range in strain space rather than in stress space. Owing to the postulated pressure independence of the elastic strain range the required evolution equation can be very simple.

In this paper, after a brief description of a hypoplastic reference model, the extension for small strains is presented. Two conceptually similar models from the literature are also briefly discussed. A new state variable, called *intergranular strain*, is presented first with a 1D model and then for 2D strain paths. Finally, a general tensor formulation is given and supplemented by some comments on numerical implementation.

The proposed extension requires five additional constants. Three of them, the size of the elastic range and two ratios of characteristic stiffnesses, have a clear physical meaning. Two exponents, related to the transition between different deformation modes (intergranular strain and grain rearrangement), appear to be universal as exponents used in the physics of second-order phase transitions. A detailed procedure for the determination of the constants is given. Finally, the performance of the extended and the original hypoplastic model is compared for some element tests.

Tensors of second order are denoted with bold letters (e.g. $\mathbf{D}$, $\mathbf{T}$, $\boldsymbol{\delta}$, $\mathbf{N}$) and tensors of fourth order with calligraphic letters (e.g. $\mathscr{L}, \mathscr{M}$). Different kinds of tensorial multiplication are used: $\mathbf{TD} = T_{ij}D_{kl}$, $\mathbf{T} : \mathbf{D} = T_{ij}D_{ij}$, $\mathscr{L} : \mathbf{D} = L_{ijkl}D_{kl}$, $\mathbf{T} \cdot \mathbf{D} = T_{ij}D_{jk}$. The Euclidean norm of a tensor is $\|\mathbf{D}\| = \sqrt{D_{ij}D_{ij}}$. Unit tensors of second and fourth order are denoted $\mathbf{1}$ (δ_{ij}) and $\mathscr{I}$($I_{ijkl} = \delta_{ik}\delta_{jl}$), respectively. Compressive stresses and strains are negative.

2. THE HYPOPLASTIC REFERENCE MODEL

Hypoplasticity is a framework for the description of mechanical behaviour of granular materials. It assumes that grains are aggregated to a so-called *simple granular skeleton* defined by the following properties:

- the state of a granular material is fully characterized by granular (effective) stress $\mathbf{T}$ and by void ratio e only;
- grains are permanent, i.e., they keep their size and general form during deformations;
- deformation of the granular skeleton is due to grain rearrangements, which are understood as relative displacements of grains including evolution and decay of grain contacts. Compression, abrasion and crushing of grains are negligible;
- surface effects (capillarity, cemented bridges, osmotic pressures) are absent;
- the deformation under homogeneous boundary conditions is homogeneous (without shear localization);
- three pressure-dependent limiting void ratios can be distinguished (Figure 1):
  - e_i represents the upper bound of the simple granular skeleton and corresponds to the

maximum void ratio during isotropic compression starting from the minimum density by pressure zero, $e > e_i$ suggests macropores and honeycomb formations;
  - e_c corresponds to the critical void ratio;[18]
  - e_d represents the lower bound of the simple granular skeleton and corresponds to the minimum void ratio after a cyclic shearing with a small amplitude, $e < e_d$ suggests a masonry-like granular skeleton;
- change of the limiting void ratios with the mean pressure is related to a so-called *granular hardness* h_s, which represents a reference pressure-independent stiffness of the soil and is the only dimensional constant in the hypoplastic equation;
- rate effects are negligible.

The hypoplastic constitutive model is generally described by a single non-linear tensorial equation that yields the stress rate $\mathring{\mathbf{T}}$ (objective, Jaumann) with the stretching rate $\mathbf{D}$:[19]

$$\mathring{\mathbf{T}} = \mathscr{L} : \mathbf{D} + \mathbf{N}\|\mathbf{D}\|. \tag{1}$$

The constitutive tensors $\mathscr{L}(\mathbf{T}, e)$ and $\mathbf{N}(\mathbf{T}, e)$ are functions of stress and void ratio. These functions are of essential importance for the quality of predictions by hypoplastic model. For completeness of this paper the mathematical representation of $\mathscr{L}(\mathbf{T}, e)$ and $\mathbf{N}(\mathbf{T}, e)$ given by von Wolffersdorff[8] is attached in Appendix A.

To satisfy the requirement of rate-independence, equation (1) is positively homogeneous of the first degree in $\mathbf{D}$. However, owing to the second term in equation (1), it is non-linear in $\mathbf{D}$, i.e., $-\mathring{\mathbf{T}}(\mathbf{D}) \neq \mathring{\mathbf{T}}(-\mathbf{D})$. The anelastic behaviour is thus achieved without the decomposition of deformation rate into an elastic and a plastic part as is usual in elasto-plasticity. Explicit formulation of yield surfaces or a flow rule is not necessary, although they can be derived from equation (1).[20]

There are seven material constants in the hypoplastic model of von Wolffersdorff.[8] All of them are closely related to the geometric and material properties of grains, and for a non-cohesive soil they can be easily determine from standard index tests.[21] Their explanation is given in Appendix A.

Now, we demonstrate briefly the major shortcoming of hypoplasticity—ratcheting. For small strain cycles in a 1D case, equation (1) can be simplified to the scalar form

$$\dot{T} = LD + N|D|; \quad 0 < -N < L. \tag{2}$$

Values of L and N can be considered constant during a cycle provided that the changes of stress and of void ratio are small. The accumulated stress in one strain cycle, $\pm\Delta\varepsilon = \pm D\Delta t$ (Figure 2(a)), is then

$$\Delta T^{\mathrm{acc}} = L\Delta\varepsilon + N|\Delta\varepsilon| + L(-\Delta\varepsilon) + N|-\Delta\varepsilon| = 2N|\Delta\varepsilon|. \tag{3}$$

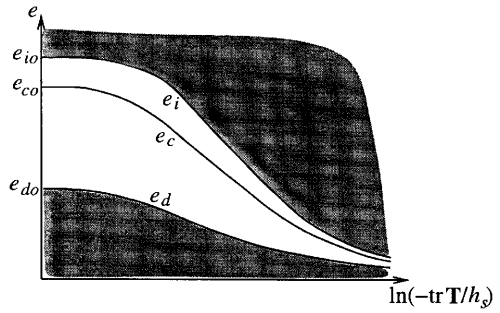

Figure 1. Pressure-dependent limiting void ratios

An accumulation of strain, viz.,

$$\Delta\varepsilon^{\mathrm{acc}} = \frac{\Delta T}{L+N} + \frac{-\Delta T}{L-N} = \frac{-2N}{L^2-N^2}\Delta T \tag{4}$$

is similarly calculated but for a small stress cycle (Figure 2(b)). In both cases the accumulation is generally too large compared with experimental results. This so-called ratcheting is typical for several constitutive models and has often been discussed in the literature[22–25] from different aspects. Our main objective in this paper is to remove the excessive ratcheting from hypoplasticity.

3. TWO OTHER SMALL-STRAIN MODELS

Among constitutive relations describing small-strain soil behaviour, we have chosen for comparison an approach with multisurface plasticity and a strain-space plasticity model, hoping that a comment might be helpful.

Stallebrass[26] has proposed an extension of the cam-clay elasto-plastic model incorporating an elastic locus and a history-dependent surface inside the bounding surface (Figure 3). Both surfaces evolve kinematically in the stress space. This model predicts the same initial stiffness after a 90° and a 180° change of the stress path direction, which contradicts experimental observations.[13] Contrary to this approach, our elastic region is formulated in strain space, history surface is not explicitly defined, and stiffness depends on the vertex angle of the strain path.

A different model has been proposed by Simpson[27] in a strain space. The behaviour of soil in a small-strain range is described by an analogy in which the strain path is represented by a walking man dragging along several bricks attached to his feet by strings of different length. (A similar model, using springs of different lengths fixed between two plates, has been proposed by Guyon and Troadec.[28]) The movements of the man correspond to the prescribed strain path and the movements of the bricks represents portions of the plastic strain rate. If all bricks are dragged along one line then the plastic strain rate is identical with the total one. Using the language of this *brick analogy*, the model proposed in our paper is constituted of a man with a single brick attached by a string of length R (Figure 4). We need fewer state variables, however, the calculations of stiffness and movements are somewhat more complicated than in Simpson's model. In our model, the motion of the brick induces stress rates according to the hypoplastic model (Figure 4(b)), whereas movements of the man with respect to the brick lead to intergranular strains with corresponding stress rates (Figure 4(a)).

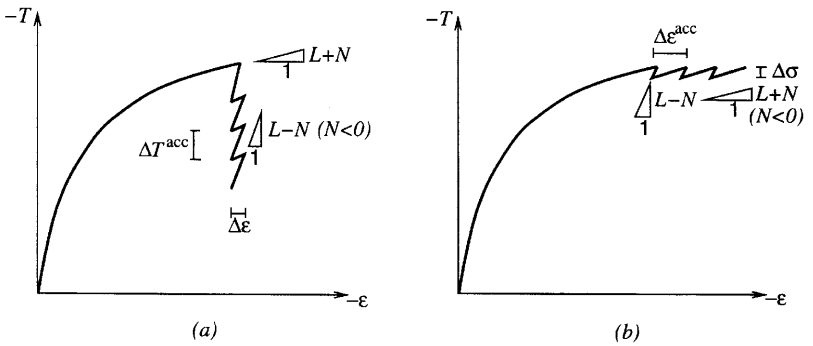

Figure 2. Excessive stress (a) and strain (b) accumulation during stress and strain cycles, respectively

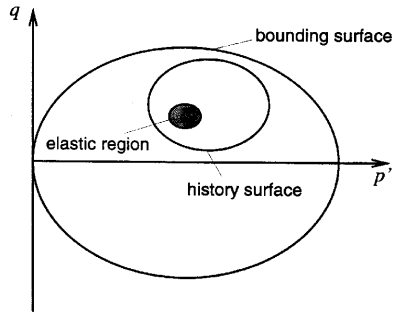

Figure 3. Three-surface model proposed by Stallebrass[26]

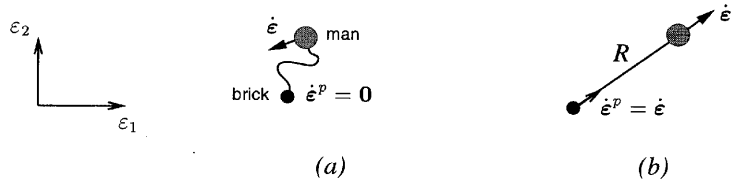

Figure 4. Brick analogue proposed by Simpson[27]

4. EXTENDED HYPOPLASTIC MODEL

Consider an element of a granular soil under such boundary conditions that its deformation can sufficiently well be described by the development of strain rate **D**. The strain is a result of (i) deformation of the intergranular interface layer and of (ii) rearrangement of the skeleton. The interface deformation is called *intergranular strain* $\boldsymbol{\delta}$ and is considered as a new state variable. Let us assume that two opposite directions of straining correspond on the micromechanical level to two opposite deformations of the interface followed by a slip on a representative contact. This simple micromechanical situation is depicted in Figure 5. The interface is represented by the shaded area. Prior to deformation we set $\delta = 0$, Figure 5(a). We may choose an arbitrary value of the deformation rate, e.g., $D = \dot{\varepsilon} = -1$. During the deformation the intergranular strain reaches its extremum $\delta = -R$, Figure 5, which cannot be surpassed by further stretching: the interface remains deformed while the grains are sliding. This sliding corresponds to a rearrangement of the grains. After a reversal of D, Figure 5(c), the deformation concentrates in the interface alone until δ passes through the original zero value, Figure 5(d). Finally δ can reach the limit $\delta = R$ on the opposite side, Figure 5(e). The intergranular strain can be understood as a macroscopic measure of microdeformations of an interface. Note that a small value of macroscopic measure may correspond to large microdeformations. The total strain results from intergranular strains and contact slips.

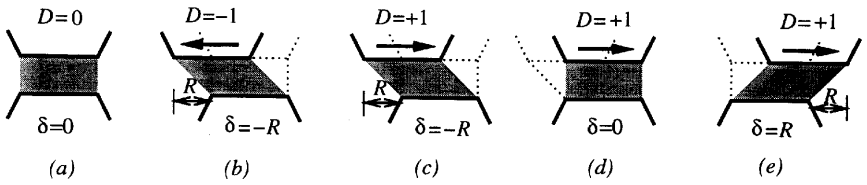

Figure 5. 1D interpretation of the intergranular strain

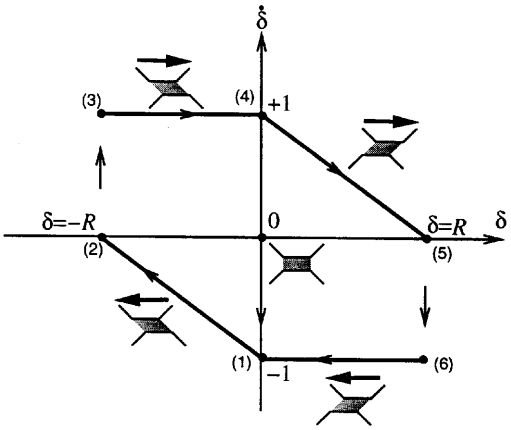

Figure 6. Evolution of δ in 1D model in a single strain cycle

In this simple model we propose a constant maximum value of intergranular strain R independently of the stress level. With increasing skeleton pressure only the intergranular contact area becomes larger, which is consistent with the explanation of dry friction as a contact adhesion[17,29,30] going back to Terzaghi.[31]

The evolution equation of δ in the above 1D model can be written as

$$\dot{\delta} = \begin{cases} \left(1 - \dfrac{|\delta|}{R}\right) D & \text{for } \delta \cdot D > 0, \\ D & \text{for } \delta \cdot D \leqslant 0. \end{cases} \tag{5}$$

A geometrical interpretation of equation (5) is shown in Figure 6. At the beginning of the deformation, the rate of intergranular strain jumps to $\dot{\delta} = D = -1$ (point 1), which means that no rearrangement of grains takes place. As $\delta \cdot D > 0$, the absolute rate of δ continuously decreases until $\delta = -R$ is reached (point 2). On further deformation in the same direction δ cannot grow any more. This corresponds to a pure rearrangement of grains. The change of the sign of D results in elastic microrebound. We have $\delta \cdot D \leqslant 0$, and $\dot{\delta} = D = +1$ (point 3) as long as $\delta \cdot D \leqslant 0$ holds (point 4). Subsequently the condition $\delta \cdot D < 0$ is fulfilled, and $\dot{\delta}$ decreases towards zero as dictated by equation (5). A cycle is closed after changing the deformation rate to $D = -1$ again (point 6) and reaching $\delta = 0$ (point 1).

In the next example the evolution of intergranular strain is demonstrated for the strain path in two-dimensional strain space, as shown in Figure 7. The evolution equation takes the form

$$\dot{\delta}_i = \begin{cases} D_i - \left(\dfrac{\delta_1 D_1 + \delta_2 D_2}{R\sqrt{\delta_1^2 + \delta_2^2}} \right) \delta_i & \text{for } \delta_k D_k > 0, \\ D_i & \text{for } \delta_k D_k \leqslant 0. \end{cases} \tag{6}$$

Let us now consider different strain paths and the corresponding changes of intergranular strain (Figure 8). The strain path (a) and the path of intergranular strain (b) for one-dimensional com-

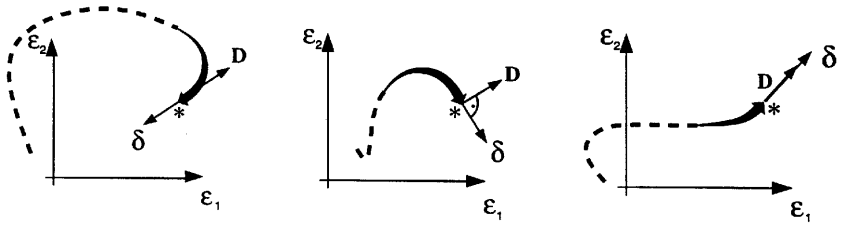

Figure 7. Different intergranular strains $\boldsymbol{\delta}$ related with different deformation histories. Only the recent part of the previous strain path (bold arrow) has an influence on $\boldsymbol{\delta}$. Current stress, void ratio and strain rate at the point * may be same in all three cases

pression and extension corresponds to the 1D model as in Figures 5 and 6. After a sharp bend (90°) of the strain path (*c*) the intergranular strain (*d*) adapts itself to the new direction of deformation, i.e.,

$$\boldsymbol{\delta} \to \mathbf{D}\frac{R}{\|\mathbf{D}\|}$$

not exceeding R. One can obtain a similar picture also for other directions of strain path (*e*), (*f*).

The asymptotic evolution of intergranular strain is similar to the asymptotic evolution of the stress path given by monotonic compression (with $\mathbf{D} = \text{constant}$), towards a straight line of constant ratio of stress components.[14] Actually we may speak of two levels of SOM-effect, one for intergranular behaviour and one for macrodeformations. Reaching the asymptotic state by grain rearrangements requires much longer proportional straining than is needed for the *intergranular* SOM-state.

In the following a more general tensorial formulation of the model will be presented with the strain rate $\mathbf{D}$ and the stress $\mathbf{T}$ being second-order tensors. The intergranular strain $\boldsymbol{\delta}$ is obtained by accumulation of $\mathbf{D}\Delta t$ so it must also be a second-order tensor.

It is convenient to denote the normalized magnitude of $\boldsymbol{\delta}$ as

$$\rho \overset{\text{def}}{=} (\|\boldsymbol{\delta}\|/R) \tag{7}$$

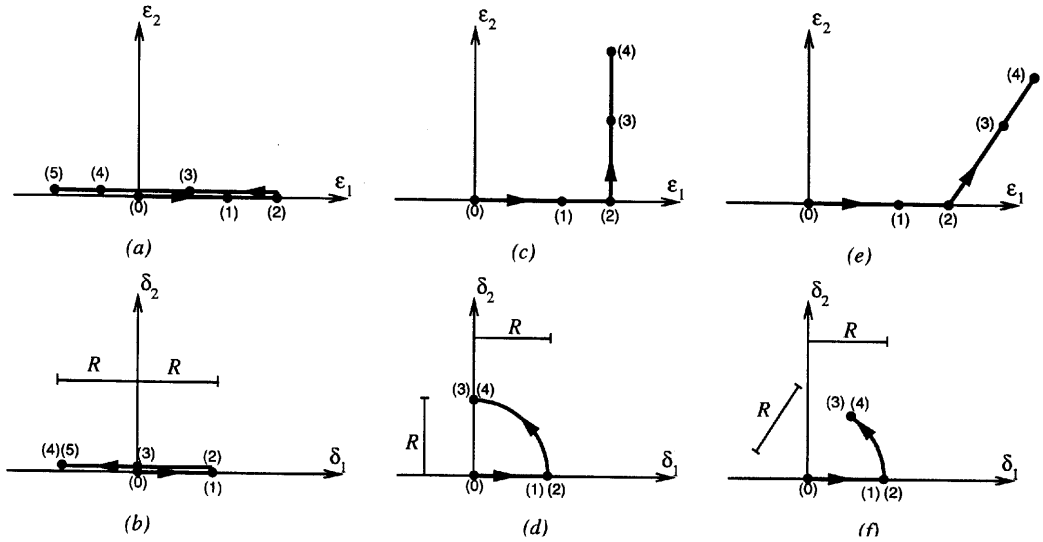

Figure 8. Strain paths and corresponding paths of intergranular strain

and the direction $\hat{\boldsymbol{\delta}}$ of intergranular strain as

$$\hat{\boldsymbol{\delta}} \stackrel{\text{def}}{=} \begin{cases} \boldsymbol{\delta}/\|\boldsymbol{\delta}\| & \text{for } \boldsymbol{\delta} \neq \mathbf{0} \\ \mathbf{0} & \text{for } \boldsymbol{\delta} = \mathbf{0} \end{cases} \tag{8}$$

We will see below that the singularity as $\|\boldsymbol{\delta}\| = 0$ is not acute numerically.

The general stress–strain relation is written as

$$\mathring{\mathbf{T}} = \mathscr{M} : \mathbf{D} \tag{9}$$

The fourth-order tensor $\mathscr{M}$ represents stiffness and is calculated from the hypoplastic tensors $\mathscr{L}(\mathbf{T}, e)$ and $\mathbf{N}(\mathbf{T}, e)$, which may be modified (increased) by scalar multipliers m_T and m_R, depending on ρ and $(\hat{\boldsymbol{\delta}} : \mathbf{D})$ as indicated in Figure 9.

We first consider the case of $\rho = 1$ (point B in Figure 9) corresponding to the maximal intergranular strain.

1. For monotonic continuation of straining with $\mathbf{D} \sim \hat{\boldsymbol{\delta}}$, we take

$$\mathscr{M} = \mathscr{L} + \mathbf{N}\hat{\boldsymbol{\delta}} \tag{10}$$

   Notice that in this case $\mathbf{D} = \hat{\boldsymbol{\delta}}\|\mathbf{D}\|$ so $\mathbf{N}\hat{\boldsymbol{\delta}} : \mathbf{D} = \mathbf{N}\|\mathbf{D}\|$ and we obtain the hypoplastic equation (1).

2. For reversed deformation, i.e. $\mathbf{D} \sim -\hat{\boldsymbol{\delta}}$, we postulate an elastic microrebound with

$$\mathscr{M} = m_R \mathscr{L} \tag{11}$$

   The multiplier m_R is a new material constant, $m_R > 1$. The second hypoplastic term unlike in equation (10) is switched off.

3. For a neutral strain rate, defined by $\mathbf{D} \perp \hat{\boldsymbol{\delta}}$ $(\mathbf{D} : \hat{\boldsymbol{\delta}} = 0)$, we postulate

$$\mathscr{M} = m_T \mathscr{L} \tag{12}$$

   with a constant m_T in the range $m_R > m_T > 1$.

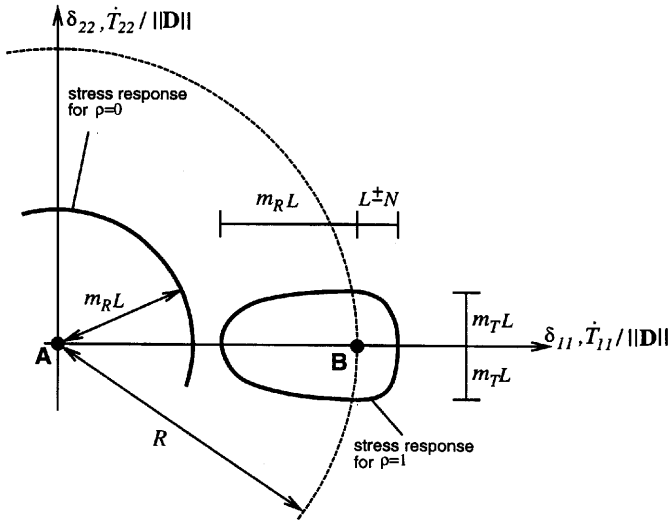

Figure 9. Modificatin of the stiffness with m_R and m_T for $\rho = 0$ and for $\rho = 1$. For simplicity this figure assumes proportionality $\dot{\mathbf{T}}(\mathbf{D}) \sim \mathbf{D}$

Next we consider the case $\rho = 0$ (point A in Figure 9) for which

$$\mathscr{M} = m_R \mathscr{L} \tag{13}$$

has been postulated. The stiffness is thus increased by factor m_R independently of the direction of $\mathbf{D}$ if $\rho = 0$.

For more general case ($0 < \rho < 1$) we calculate stiffness $\mathscr{M}$ using the following interpolation

$$\mathscr{M} = [\rho^{\chi} m_T + (1 - \rho^{\chi}) m_R]\mathscr{L} + \begin{cases} \rho^{\chi}(1 - m_T)\mathscr{L} : \hat{\boldsymbol{\delta}}\hat{\boldsymbol{\delta}} + \rho^{\chi}\mathbf{N}\hat{\boldsymbol{\delta}} & \text{for } \hat{\boldsymbol{\delta}} : \mathbf{D} > 0 \\ \rho^{\chi}(m_R - m_T)\mathscr{L} : \hat{\boldsymbol{\delta}}\hat{\boldsymbol{\delta}} & \text{for } \hat{\boldsymbol{\delta}} : \mathbf{D} \leqslant 0 \end{cases} \tag{14}$$

In order to obtain the special cases mentioned above, we may substitute $\hat{\boldsymbol{\delta}}\hat{\boldsymbol{\delta}} : \mathbf{D} = \mathbf{D}$ and $\hat{\boldsymbol{\delta}} : \mathbf{D} = \|\mathbf{D}\|$ for $\mathbf{D} \sim \hat{\boldsymbol{\delta}}$ and of course $\hat{\boldsymbol{\delta}} : \mathbf{D} = 0$ for $\mathbf{D} \perp \hat{\boldsymbol{\delta}}$. The transition from $m_R\mathscr{L}$ to $\mathscr{L} + \mathbf{N}\hat{\boldsymbol{\delta}}$ for $0 < \rho < 1$ is smoothed by a weighting factor ρ^{χ}, wherein χ is a constant.

Immediately after a full (180°) strain reversal the stiffness $m_R\mathscr{L}$ is the largest possible one for a given stress and void ratio. It remains so as long as $\hat{\boldsymbol{\delta}} : \mathbf{D} \leqslant 0$. Intergranular strain $\boldsymbol{\delta}$ changes in this case identically with macroscopic strain. In this case the grain skeleton is fixed and hypoplasticity is 'switched off': the term $\mathbf{N}\hat{\boldsymbol{\delta}}$ does not appear in equation (14) for $\hat{\boldsymbol{\delta}} : \mathbf{D} \leqslant 0$. As soon as $\hat{\boldsymbol{\delta}} : \mathbf{D}$ becomes positive the intergranular strain starts to grow and the stiffness decreases down to the hypoplastic value $\mathscr{L} + \mathbf{N}\hat{\boldsymbol{\delta}}$ while the intergranular strain grows up to $\|\boldsymbol{\delta}\| = R$.

Generalizing equation (6), we obtain the evolution equation for the intergranular strain tensor $\boldsymbol{\delta}$. With the aid of Figure 10, we postulate

$$\mathring{\boldsymbol{\delta}} = \begin{cases} (\mathscr{I} - \hat{\boldsymbol{\delta}}\hat{\boldsymbol{\delta}}\rho^{\beta_r}) : \mathbf{D} & \text{for } \hat{\boldsymbol{\delta}} : \mathbf{D} > 0 \\ \mathbf{D} & \text{for } \hat{\boldsymbol{\delta}} : \mathbf{D} \leqslant 0 \end{cases} \tag{15}$$

where $\boldsymbol{\delta}$ is the objective rate of intergranular strain (see Appendix C). The exponent β_r is a material constant which (for simplicity) was assumed equal to one in equation (6).

Consider now the evolution equation of intergranular strain. According to equation (15), during a monotonic deformation with $\mathbf{D} =$ constant we have $\lim_{t\to\infty} \boldsymbol{\delta} = \mathbf{D}R/\|\mathbf{D}\|$. If $\hat{\boldsymbol{\delta}} : \mathbf{D} > 0$ and $\rho = 1$ then the intergranular interfaces remain deformed during a proportional straining with $\boldsymbol{\delta} = \mathbf{D}R/\|\mathbf{D}\| =$ constant and stress rate can be calculated from hypoplastic equation (equation (9) with (14) becomes identical to (1)). In the case of a sudden change of the direction of straining (by less than 90°) $\boldsymbol{\delta}$ rotates towards the new $\mathbf{D}$ keeping $\rho = 1$. Indeed, after perusal of equation (15) we see that for $\rho = 1$ only the neutral part $\mathbf{D} - \hat{\boldsymbol{\delta}}\hat{\boldsymbol{\delta}} : \mathbf{D}$ contributes to the evolution of $\boldsymbol{\delta}$ so that ρ remains constant. For $\rho = 0$, we have $\boldsymbol{\delta} = \mathbf{D}$ independent of the direction of $\mathbf{D}$. Actually, equation (15) can be seen as a kind a power law interpolation (with ρ^{β_r}) between the special cases $\rho = 0$ and $\rho = 1$ (Figure 11).

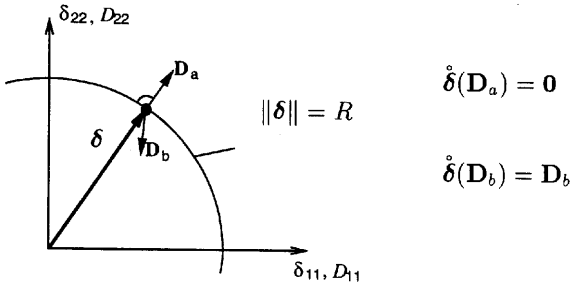

Figure 10. Rate of the intergranular strain for the special case $\rho = 1$. According to equation (15) the rate $\hat{\boldsymbol{\delta}}$ vanishes in the case of $\mathbf{D}_a = \hat{\boldsymbol{\delta}} \parallel \mathbf{D}_a \parallel (\hat{\boldsymbol{\delta}} : \mathbf{D}_a > 0)$, and $\hat{\boldsymbol{\delta}} = \mathbf{D}$ in the case of $\mathbf{D}_b (\hat{\boldsymbol{\delta}} : \mathbf{D}_b < 0)$

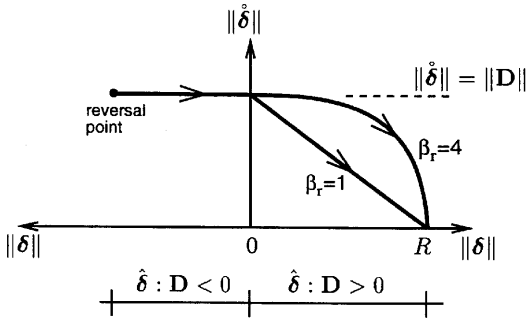

Figure 11. Evolution of the intergranular strain $\boldsymbol{\delta}$. After a 180° strain reversal $\mathbf{D}$ is assumed to remain constant. At first $\mathbf{D} \sim -\hat{\boldsymbol{\delta}}$ so $\dot{\boldsymbol{\delta}} = \mathbf{D}$, then $\mathbf{D} \sim \hat{\boldsymbol{\delta}}$ so $\|\boldsymbol{\delta}\|$ decreases according to equation (15)

The stress response $\mathring{\mathbf{T}}(\mathbf{D})$ of the model is continuous if plotted over the direction of an applied strain but the stiffness $\partial\mathring{\mathbf{T}}/\partial\mathbf{D}$ is not (see equation (14)). Thus, the extended constitutive model presented above is not strictly hypoplastic in the sense of the definition given by Wu and Kolymbas.[32]

The linear part of the model is hypo-elastic so is not necessarily conservative. If desired, $\mathscr{L}$ can be replaced by a *hyper*-elastic stiffness. An appropriate formulation can be found elsewhere, e.g., References 3 and 33.

5. NUMERICAL ASPECTS

Consider numerical element tests with stress or mixed control. Solving the constitutive equation (14) is more complicated than the purely hypoplastic relation, because the new relation is bilinear, and the sign of $\hat{\boldsymbol{\delta}} : \mathbf{D}$ has to be tested in all increments.

Unless $\mathbf{D}$ is given directly, we have to solve the auxiliary equation

$$\mathring{\mathbf{T}} = \mathscr{L} : \mathbf{D}^* \tag{16}$$

instead of equation (9) for $\mathbf{D}^*$, where $\mathbf{D}^*$ is an estimate of the strain rate. In stress-controlled problems all components of $\mathring{\mathbf{T}}$ are given and $\mathbf{D}^*$ can be obtained from equation (16). A unique strain rate $\mathbf{D}$ can then be found for a given stress rate $\mathring{\mathbf{T}}$ from equations (9) and (14), provided it is unique for the non-extended version of hypoplasticity $\mathring{\mathbf{T}} = \mathscr{L} : \mathbf{D} + \mathbf{N}\|\mathbf{D}\|$.

For a mixed control, some components of $\mathbf{D}$ and some components of $\mathring{\mathbf{T}}$ are given. In this case, first, equation (16) must be solved for the unknown components of $\mathbf{D}^*$. The estimation of $\mathbf{D}^*$ suffices (in place of $\mathbf{D}$) to determine the sign $\hat{\boldsymbol{\delta}} : \mathbf{D}$, being identical with the one of $\hat{\boldsymbol{\delta}} : \mathbf{D}^*$. For proof of this fact and for discussion of the uniqueness of solution of mixed problems see Appendix B. Having the sign of $\hat{\boldsymbol{\delta}} : \mathbf{D}$, we may proceed with solving a mixed problem using equation (9) with an appropriate $\mathscr{M}$ given by equation (14).

An automatic incrementation algorithm should be used in numerical calculations with the proposed model. Especially, directly after sharp reversals of strain paths unusually small increments must be used. The strain increments used in the following numerical calculations are chosen as $\Delta\varepsilon \approx 0.001$ for $\hat{\boldsymbol{\delta}} : \mathbf{D} > 0$ and smaller than $0{\cdot}2R$ for $\hat{\boldsymbol{\delta}} : \mathbf{D} < 0$ in order to secure numerical stability. The recommended maximum $\Delta\varepsilon$ during $\hat{\boldsymbol{\delta}} : \mathbf{D} > 0$ can be calculated from equation (15) as

$$\Delta\varepsilon_{\max} = \frac{\mu R}{1 - \rho^{\beta r}} \tag{17}$$

where $0 < \mu < 1$ is a parameter that controls the magnitude of the increment $\Delta\varepsilon_{\max}$ (we propose $\mu = 0.2$). However, even so small increments cause some second-order errors. In classical stress-space elasto-plastic models the necessary correction is usually made by projecting the updated stress onto the updated yield surface. In the case of our strain-space formulation for $\rho > 1$ it is preferable to correct $\boldsymbol{\delta}$ rather than to modify the actual strain.

Although some correction of $\boldsymbol{\delta}$ may follow automatically in next time-steps due to the $\rho^{\beta r}$ term in equation (15), we do not recommend to rely on this 'self-healing' property of the evolution equation in predictions of cyclic response.

An updated Lagrange formulation with an explicit Euler time integration scheme seems appropriate. Then we have

$$\mathbf{T}_{t+\Delta t} = \mathbf{T}_t + \dot{\mathbf{T}}_t \Delta t \tag{18}$$

whereby $\dot{\mathbf{T}}_t$ is calculated using the stress state $\mathbf{T}_t$ and the void ratio e_t at the beginning of an increment. In general, the Jaumann term $(-\mathbf{W}\cdot\mathbf{T} + \mathbf{T}\cdot\mathbf{W})\Delta t$ has to be included. The same should be done when updating $\boldsymbol{\delta}$, see Appendix C.

The Jacobian (stiffness) matrix, $\partial\Delta\mathbf{T}/\partial\Delta\boldsymbol{\epsilon}$, can be calculated assuming that the next strain increment is proportional to the current one. One should avoid the updating of state variables during equilibrium iteration because of the danger of non-physical (numerical) reversals.

6. DETERMINATION OF THE ADDITIONAL CONSTANTS

The maximum value of intergranular strain can be found from stress–strain curves obtained either from so-called dynamic tests or from static tests with strain reversals. The incremental stiffness remains approximately constant within a certain strain range there. The size of this range can be identified with the constant R (Figure 12).

In order to determine the constants m_T and m_R in equation (14), we recommend comparative tests at fixed values of $\mathbf{T}$, e and $\mathbf{D}$ but with different $\boldsymbol{\delta}$, i.e., with different recent deformation histories. Intergranular strains $\boldsymbol{\delta}$ induced by various recent strain histories have been already depicted in Figure 7. The asterisks in Figure 7 correspond to the starting point ($\boldsymbol{\epsilon} = \mathbf{0}$) of the stiffness–strain curves in Figure 12 for which $\mathbf{T}$, e and $\mathbf{D}$ are the same. During monotonic deformation (a) the stiffness E_0 may slowly change (here decrease) also due to the general $E_0(\mathbf{T})$ dependence. After a 90° reversal of the strain path (b) the stiffness decreases starting from E_T down to E_0, and after a 180° strain reversal (c) from E_R to E_0. All three stiffnesses approximately coincide at $\varepsilon = \varepsilon_{\mathrm{SOM}}$. Small discrepancies in stiffness at $\varepsilon = \varepsilon_{\mathrm{SOM}}$ are caused by a different *stresses*. Note that $\mathbf{T}$ and e are identical only for $\boldsymbol{\epsilon} = \mathbf{0}$

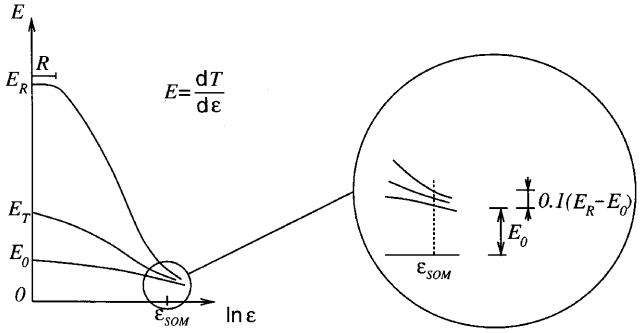

Figure 12. Characteristic stiffness values for the model calibration

and not for the whole strain path of interest. The increase in stiffness is modelled by the constants m_T and m_R. They can be measured from a series of strain controlled tests with $\mathbf{D} = \text{constant}$ (e.g., plane strain tests[34]) starting from a given stress, void ratio but preceded by different recent deformation histories.

The parameter β_r influences the evolution of intergranular strain and can be correlated with the length $\varepsilon_{\mathrm{SOM}}$ of the straight strain path, measured from the reversal point to the point where the additional stiffness becomes by definition less than 10% of its value directly after reversal, see Figure 12.

We approximate the upper curve in Figure 12 as

$$E = \begin{cases} m_R E_0 \quad (= E_R) & \text{for } \varepsilon < R \\ E_0 + E_0(m_R - 1)[1 - \rho^{\chi}] & \text{for } \varepsilon > R \end{cases} \tag{19}$$

which follows directly from equation (14) for $\mathbf{D} \sim \boldsymbol{\delta}$ and with $\mathbf{N} = \mathbf{0}$. The dependence of ρ on $\boldsymbol{\delta}$ can be found for $\varepsilon > R$ from (7) and (15) under assumption of a 1D monotonic path with $\dot{\varepsilon} \sim \hat{\delta}$ and $\dot{\varepsilon} : \hat{\delta} > 0$. The resulting ordinary differential equation

$$\frac{\mathrm{d}\rho}{\mathrm{d}\varepsilon} = (1 - \rho^{\beta r})/R \tag{20}$$

can be solved for the known boundary conditions $\rho^{\chi}|_{\varepsilon=R} = 0$ and $\rho^{\chi}|_{\varepsilon=\varepsilon_{\mathrm{SOM}}} = 0.9$. In our solutions we disregard the dependence E_0 on $\mathbf{T}$ for $0 < \varepsilon < \varepsilon_{\mathrm{SOM}}$.

The solution of equation (20) can be presented for different χ in the form of a diagram, see Figure 13. For example, for $\chi = 6, R = 0{\cdot}0001$ and $\varepsilon_{\mathrm{SOM}}/R \approx 8$ we obtain from this diagram $\beta_r \approx 0{\cdot}50$.

The parameter $\chi(\chi > 1)$ describes the degradation of the stiffness from E_R to E_0 during monotonic deformation. Equation (14) provides a smooth transition from $E_R(= m_R L)$ to the hypoplastic stiffness $E_0 = L \pm N$ as ρ changes from 0 to 1. The parameter χ can be calibrated from cyclic test with small strain amplitudes. The stress accumulated during a single strain cycle of the amplitude $\Delta\varepsilon_A$ is a function of χ and β_r. Consider a series of small strain cycles such that $\mathbf{T}$ and e remain nearly constant as well as $\mathscr{L}$ and $\mathbf{N}$. Owing to the evolution equation (15), after a number of cycles a kind of stable state is achieved in which $\boldsymbol{\delta}$ oscillates periodically around $\boldsymbol{\delta} = \mathbf{0}$ with the amplitude $\pm\delta_A$ (Figure 14).

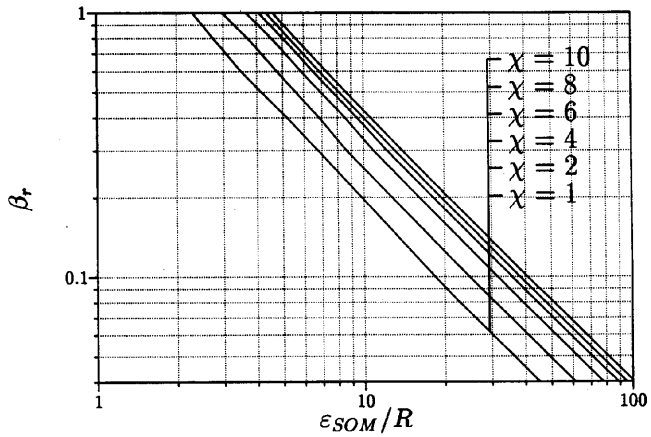

Figure 13. Correlation of β_r versus $\varepsilon_{\mathrm{SOM}}/R$ for different χ

This can be considered as a kind of micro shakedown. The accumulation of stress after one cycle (cf. equation (3)) is then

$$\Delta\mathbf{T}^{\mathrm{acc}} = 2\mathbf{N}R\int_0^{\rho A}\frac{\rho^{\chi}}{1-\rho^{\beta r}}\mathrm{d}\rho \tag{21}$$

The maximum intergranular strain during such a cyclic deformation is $\delta_A = R\cdot\rho_A$. The relation between ρ_A and the straining amplitude ε_A can be found from (7) and (15) as

$$2\frac{\varepsilon_A}{R} - \rho_A - \int_0^{\rho_A}\frac{\mathrm{d}\rho}{1-\rho^{\beta}r} = 0 \tag{22}$$

Equations (21) and (22) must be solved numerically for different β_r. The results are plotted in diagrams (Figure 15).

In order to find χ, one can perform a cyclic strain test and measure the stress response. E.g., during undrained cycles with a small amplitude of axial strain ε_A = constant we observe a decrease in the vertical stress with each cycle. Having measured $\Delta\mathbf{T}^{\mathrm{acc}}$ at the given ε_A, the corresponding value of χ can be found from Figure 15 (only the cases $\beta_r = 0{\cdot}05$ and $\beta_r = 0{\cdot}5$ have been shown there).

7. NUMERICAL SIMULATION OF ELEMENT TESTS

The performance of the extended hypoplastic model is compared now with the reference version (see Section 2). The hypoplastic constants in Table I have been found for Hochstetten sand from the vicinity of Karlsruhe, Germany.[8,35]

We assume that the intergranular strain tends to zero after some resting period. According to Jardine, Symes and Burland[11] an increase of stiffness is observed after strain reversals as well as after a 'resting period'. In order to take this second phenomenon into account one could introduce a slow monotonic change of $\boldsymbol{\delta}$ towards zero, e.g. $\overset{\circ}{\boldsymbol{\delta}} = -k\boldsymbol{\delta}$, with k being a positive scalar function of time. As long as this process is not sufficiently recognized we prefer simply to set $\boldsymbol{\delta} = 0$ after each resting period. We argue that the pure resting period is a mathematical simplification only and there are always some small movements. According to equation (15) such small cyclic changes of $\boldsymbol{\epsilon}$ make $\boldsymbol{\delta}$ drift towards zero.

Using the constants in Table I, an influence of the recent deformation history on the stiffness has been numerically calculated and depicted in Figure 16. The tangential stiffness $G_t = \mathrm{d}(T_1 - T_2)/\mathrm{d}(\varepsilon_1 - \varepsilon_2)$ has been computed after a change in direction of straining according to Figure

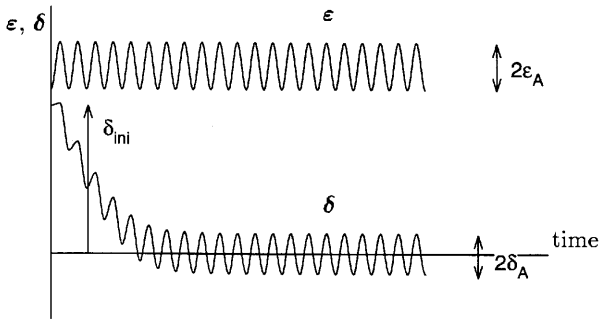

Figure 14. Evolution of $\boldsymbol{\delta}$ for strain cycles with a small amplitude ε_A. The unsymmetry of intergranular strain $\boldsymbol{\delta}$ gradually dwindles with the number of cycles

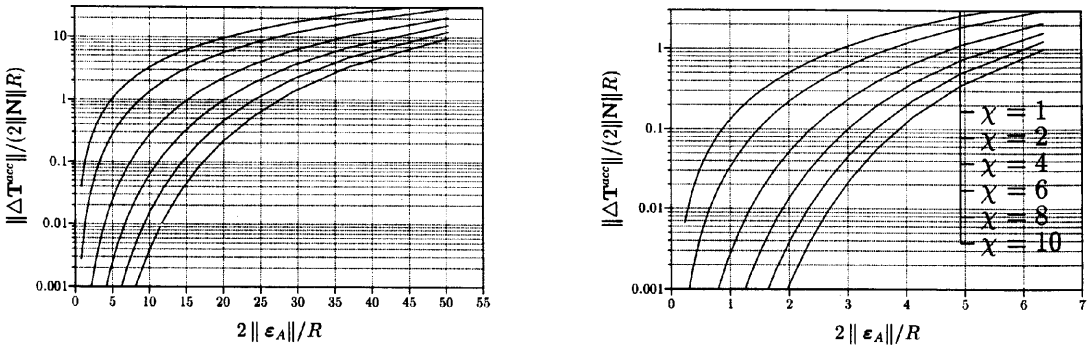

Figure 15. Relation between the strain amplitude and the accumulated stress in one-half of the strain cycle for different χ; $\beta_r = 0{\cdot}05$ (left) and $\beta_r = 0{\cdot}5$ (right)

Table I. Hypoplastic parameters of Hochstetten sand

$\varphi(^\circ)$	h_s(MPa)	n	e_{c0}	e_{d0}	e_{i0}	α	R	m_R	m_T	β_r	χ
33	1 000	0·25	0·95	0·55	1·05	0·25	1×10^{-4}	5·0	2·0	0·50	6·0

7. The state in Figure 7 corresponds to the isotropic stress $T = -100$ kN/m^2 and the void ratio $e_0 = 0{\cdot}695$. The deformation corresponds to biaxial (plane strain) compression with constant volume.

There is a distinct elastic range with the higher stiffness after the strain path reversal (180°). All three curves coincide at strain of ca. 10^{-3} which may be taken as $\varepsilon_{\mathrm{SOM}}$, i.e., at this strain the previous deformation history is swept out from the material memory. The dotted curve does not exactly coincide with the lower ones because of the dependence of G on $\mathbf{T}$ (stresses at $\varepsilon_{\mathrm{SOM}}$ are different).

Stress cycles during a one-dimensional (oedometric) compression test in the overconsolidated range show a much smaller accumulation of compaction (see Figure 17 left) as compared with the pronounced ratcheting of the stress–strain curves from the reference hypoplastic model (in Figure 17 right) for this type of deformation.

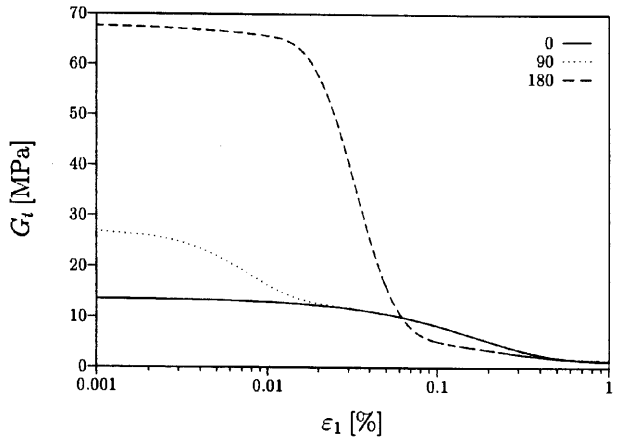

Figure 16. Calculated stiffness $G_t = \mathrm{d}(T_1 - T_2)/\mathrm{d}(\varepsilon_1 - \varepsilon_2)$ for a biaxial compression with constant volume after a change of strain path direction

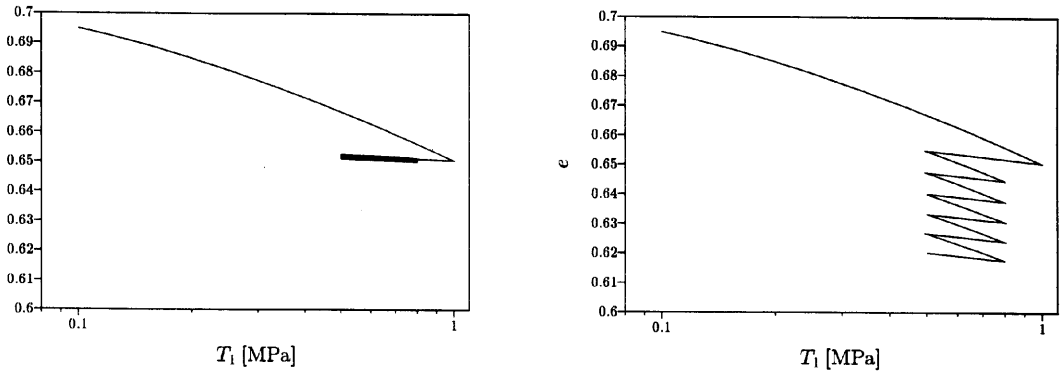

Figure 17. Oedometric compression (left: extended model, right: reference model)

The ratcheting of the stress–strain curve of the reference hypoplastic model in calculation of a triaxial drained compression test (Figure 18 right) is overcome with the extended model (Figure 18 left).

Cyclic undrained triaxial shearing leads to a build-up of pore pressure and a corresponding decrease of effective stress. For medium-dense to dense granular material a so-called cyclic mobility can be reached. It is characterized by a 'butterfly'-like trajectory in the stress space at a growing strain amplitude. Though this butterfly attractor itself is fairly well modelled by the reference version of hypoplasticity it is approached too fast. Two examples are given in Figures 19 and 20 for unsymmetric and symmetric deviatoric stress cycles respectively. The calculation was performed for the initial void ratio $e_0 = 0{\cdot}695$ and initially isotropic pressure $p' = 0{\cdot}3$ MPa.

The number of undrained stress cycles sustained by the sample prior to cyclic mobility may be practically important. The results for symmetric deviatoric stress cycles are shown in Figure 21. The relation obtained in the numerical calculations coincides qualitatively with the experimental results in Reference 36. From Figure 21 it is also apparent that the reference hypoplastic model predicts too small a number of cycles, especially for low stress amplitudes.

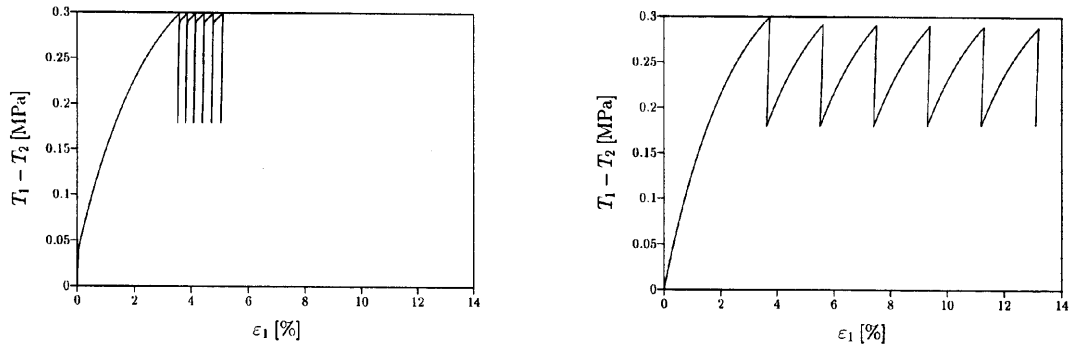

Figure 18. Drained triaxial compression with the same deviatoric stress cycles (left: extended model, right: reference model)

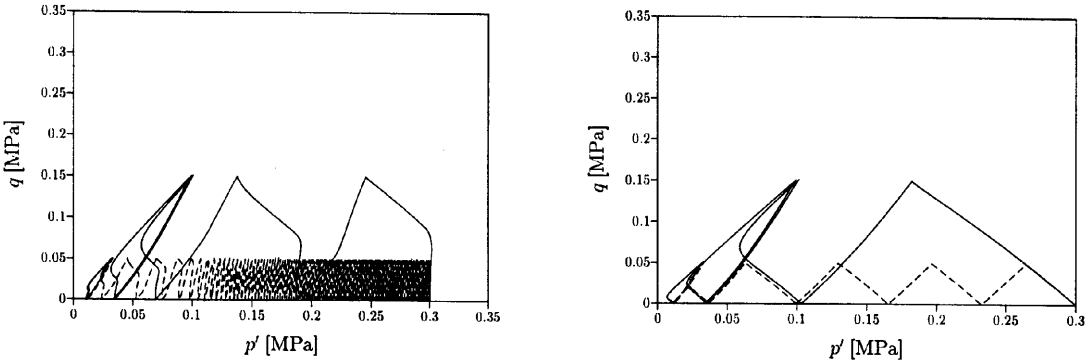

Figure 19. Undrained triaxial compression with unsymmetric deviatoric stress cycles of different amplitude (left: extended model, right: reference model). $p' = T_{ii}/3$ denotes the effective mean pressure, q is the stress deviator

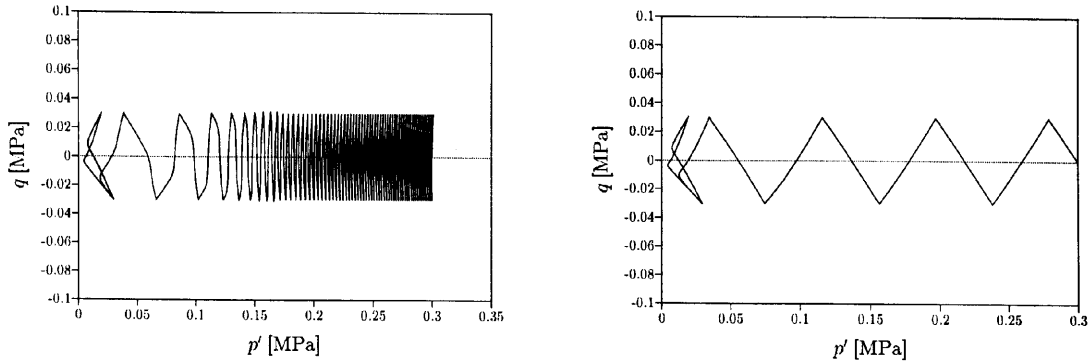

Figure 20. Undrained triaxial compression with symmetric deviatoric stress cycles (left: extended model, right: reference model)

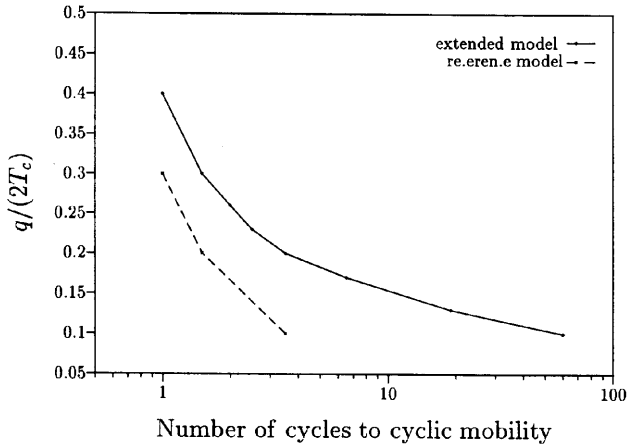

Figure 21. Number of cycles to cyclic mobility in undrained triaxial compression with symmetric deviatoric stress cycles of different amplitudes $q/(2T_c)$. T_c is the cell pressure and q the stress deviator

ACKNOWLEDGEMENTS

The authors are grateful to Prof. Gudehus for stimulating discussions, careful reading of the manuscript and many valuable remarks.

APPENDIX A

We use a version of the hypoplastic model recently published by von Wolffersdorff.[8] Its mathematical formulation can be summarized as follows:

$$\mathscr{L} = f_b f_e \frac{1}{\hat{\mathbf{T}} : \hat{\mathbf{T}}} (F^2 \mathscr{I} + a^2 \hat{\mathbf{T}} \hat{\mathbf{T}}) \tag{23}$$

$$\mathbf{N} = f_d f_b f_e \frac{Fa}{\hat{\mathbf{T}} : \hat{\mathbf{T}}} (\hat{\mathbf{T}} + \hat{\mathbf{T}}^*) \tag{24}$$

$$\hat{\mathbf{T}} \overset{\text{def}}{=} \mathbf{T}/\mathrm{tr}\mathbf{T}, \ \hat{\mathbf{T}}^* \overset{\text{def}}{=} \hat{\mathbf{T}} - \tfrac{1}{3}\mathbf{1} \tag{25}$$

$$a \overset{\text{def}}{=} \frac{\sqrt{3}(3 - \sin\varphi_c)}{2\sqrt{2}\sin\varphi_c} \tag{26}$$

$$F \overset{\text{def}}{=} \sqrt{\frac{1}{8}\tan^2\psi + \frac{2 - \tan^2\psi}{2 + \sqrt{2}\tan\psi\cos 3\theta}} - \frac{1}{2\sqrt{2}}\tan\psi \tag{27}$$

$$\tan\psi \overset{\text{def}}{=} \sqrt{3}\|\hat{\mathbf{T}}^*\|, \ \cos 3\theta \overset{\text{def}}{=} -\sqrt{6}\frac{\mathrm{tr}(\hat{\mathbf{T}}^* \cdot \hat{\mathbf{T}}^* \cdot \hat{\mathbf{T}}^*)}{[\hat{\mathbf{T}}^* : \hat{\mathbf{T}}^*]^{3/2}} \tag{28}$$

For $\hat{\mathbf{T}}^* = \mathbf{0}$ is $F = 1$. The parameter φ_c corresponds to the critical friction angle. The development of equation (23) can be found elsewhere.[1,2,37,38]

The scalar factors $f_b \cdot f_e$ and f_d take into account the influence of mean pressure and density:[6,7]

$$f_b f_e \overset{\text{def}}{=} \frac{h_s}{n}\frac{1 + e_i}{e}\left(\frac{-\mathrm{tr}\mathbf{T}}{h_s}\right)^{1-n}\left[3 + a^2 - a\sqrt{3}\left(\frac{e_{i0} - e_{d0}}{e_{c0} - e_{d0}}\right)^{\alpha}\right]^{-1} \tag{29}$$

$$f_d \overset{\text{def}}{=} \left(\frac{e - e_d}{e_c - e_d}\right)^{\alpha} \tag{30}$$

Three characteristic void ratios—e_i (during isotropic compression at the minimum density), e_c (critical void ratio) and e_d (maximum density)—decrease with mean pressure according to a relation by Bauer,[7] see Figure 1:

$$\frac{e_i}{e_{i0}} = \frac{e_c}{e_{c0}} = \frac{e_d}{e_{d0}} = \exp\left[-\left(\frac{-\mathrm{tr}\mathbf{T}}{h_s}\right)^n\right] \tag{31}$$

The range of admissible void ratios is limited by e_i and e_d.

The constants of the hypoplastic relation can be determined from simple tests:[21]

1. φ_c, critical (residual) friction angle, corresponds to the angle of repose of a loose soil.
2. e_{c0}, is identical to the conventional maximum void ratio $e_{\max}$ or with critical e_c for continued granular flow at vanishing pressure.
3. e_{d0}, is identical to the conventional minimum void ratio $e_{\min}$ obtained by shaking.

4. h_s, granular hardness, is a pressure-independent stiffness that for sands can be estimated from mean grain size d_{50} and uniformity C_u, or precisely determined from an oedometer test.
5. An exponent n, appearing in the power law for proportional compression,39 is close to 0·30 for many sands.
6. An exponent α, can be estimated from d_{50} and C_u, or calculated from the triaxial peak friction angle at a given pressure and density.
7. e_{i0}, is a maximum possible void ratio at zero pressure; $e_{i0} = 1{\cdot}1e_{c0}$ can be often assumed.

The relation between the Cauchy stress rate $\dot{\mathbf{T}}$ and the objective (Jaumann) stress rate $\mathring{\mathbf{T}}$ is

$$\dot{\mathbf{T}} = \mathring{\mathbf{T}} + \mathbf{W}\cdot\mathbf{T} - \mathbf{T}\cdot\mathbf{W} \tag{32}$$

where $\mathbf{W}$ denotes the spin tensor.[19]

APPENDIX B

There are two formulae for $\mathring{\mathbf{T}}$ in our constitutive model: one for $\hat{\boldsymbol{\delta}}:\mathbf{D} > 0$ and one for $\hat{\boldsymbol{\delta}}:\mathbf{D} \leqslant 0$. If the stress rate $\mathring{\mathbf{T}}$ is prescribed and we have to solve (9) for $\mathbf{D}$, it is not obvious which equation should be taken to calculate $\mathbf{D}$ and whether there always exists a unique solution of such a problem. We demonstrate that the approximation $\mathbf{D}^*$ obtained from (16) suffices to distinguish between $\hat{\boldsymbol{\delta}}:\mathbf{D} > 0$ and $\hat{\boldsymbol{\delta}}:\mathbf{D} < 0$.

We use the decomposition $\mathbf{D} = \mathbf{D}^n + \mathbf{D}^t$, given by

$$\mathbf{D}^n = \hat{\boldsymbol{\delta}}\hat{\boldsymbol{\delta}}:\mathbf{D};\ \ \mathbf{D}^t = (\mathscr{I} - \hat{\boldsymbol{\delta}}\hat{\boldsymbol{\delta}}):\mathbf{D} \tag{33}$$

Normal and tangential parts of $\mathbf{D}$ refer to the surface $\|\boldsymbol{\delta}\| = R$ shown in Figure 10 ($\mathbf{D}^n \| \hat{\boldsymbol{\delta}}$, $\mathbf{D}^t \perp \hat{\boldsymbol{\delta}}$).

The stress response can be expressed as a sum of the responses to $\mathbf{D}^t$ and to $\mathbf{D}^n$

$$\mathring{\mathbf{T}} = \mathring{\mathbf{T}}(\mathbf{D}^n) + \mathring{\mathbf{T}}(\mathbf{D}^t) = a\mathscr{L} : \mathbf{D}_n + b\mathscr{L} : \mathbf{D}^t + c\mathbf{N}\hat{\boldsymbol{\delta}}:\mathbf{D}^n \tag{34}$$

where

$$a = (1-\rho^\chi)m_R + \begin{cases} \rho^\chi & \text{for } \hat{\boldsymbol{\delta}}:\mathbf{D} > 0 \\ \rho^\chi m_R & \text{for } \hat{\boldsymbol{\delta}}:\mathbf{D} \leqslant 0 \end{cases} \tag{35}$$

$$b = \rho^\chi m_T + (1-\rho^\chi)m_R \tag{36}$$

$$c = \begin{cases} \rho^\chi & \text{for } \hat{\boldsymbol{\delta}}:\mathbf{D} > 0 \\ 0 & \text{for } \hat{\boldsymbol{\delta}}:\mathbf{D} \leqslant 0 \end{cases} \tag{37}$$

Assume first that the solution of (34) is unique for all $\mathring{\mathbf{T}}$ (this assumption will be proven further). The test of sign($\hat{\boldsymbol{\delta}}:\mathbf{D}$) can then be performed not necessarily with $\mathbf{D}$ but also with any

$$\mathbf{D}^* = a^*\mathbf{D}^n + b^*\mathbf{D}^t \tag{38}$$

where $a^* > 0$ and b^* is any number. We limit ourselves to the case of condition equivalent $\hat{\boldsymbol{\delta}}:\mathbf{D} \leqslant 0$ since the opposite case results automatically. The constitutive equation takes the form

$$\mathring{\mathbf{T}} = \mathscr{M} : \mathbf{D} = a\mathscr{L} : \mathbf{D}_n + b\mathscr{L} : \mathbf{D}^t \tag{39}$$

We choose $a^* = a$ and $b^* = b$ so that equation (34) takes the simple form

$$\mathring{\mathbf{T}} = a\mathscr{L} : \mathbf{D}^n + b\mathscr{L} : \mathbf{D}^t + \mathscr{L} : \mathbf{D}^* \tag{40}$$

With limitation $m_R > 0$ and $0 < \rho < 1$ the value of a is positive, so the product $\hat{\boldsymbol{\delta}}:\mathbf{D}^*$ gives the true sign of $\hat{\boldsymbol{\delta}}:\mathbf{D}$.

Next we have to prove the uniqueness of the solution of equation (34) for $\mathbf{D}$. The uniqueness will be lost if there exists $\mathbf{D}^1 \neq \mathbf{D}^2$ such that $\mathring{\mathbf{T}}^1 = \mathring{\mathbf{T}}^2$. If both $\mathbf{D}^1$ and $\mathbf{D}^2$ belong to the same regime, that is, if $\text{sign}(\hat{\boldsymbol{\delta}}:\mathbf{D}^1) = \text{sign}(\hat{\boldsymbol{\delta}}:\mathbf{D}^2)$, the stiffness $\mathscr{M}$ in both cases is identical and the solution of such a linear system is unique ($\mathbf{D}^1 = \mathbf{D}^2$). Owing to the imposed continuity of the stress response, the stress rates corresponding to the tangential strain rate $\mathbf{D}^t$ are for both regimes equal. According to the assumed superposition (34), it is therefore sufficient to consider $\mathbf{D}^n$ only. Without loss of generality we may investigate $\mathbf{D}^1 = \hat{\boldsymbol{\delta}}$ and $\mathbf{D}^2 = -\xi^2\hat{\boldsymbol{\delta}}$ with ξ being any real number. If a non-unique solution exists, the difference of the respective stress rates must vanish

$$a\mathscr{L} : \mathbf{D}^1 + c\mathbf{N}\hat{\boldsymbol{\delta}}:\mathbf{D}^1 - a'\mathscr{L} : \mathbf{D}^2 = \mathscr{L} : \hat{\boldsymbol{\delta}}(a + a'\xi^2) + c\mathbf{N} = \mathbf{0} \tag{41}$$

wherein $a = (1 - \rho^\chi)m_R + \rho^\chi$ and $a' = (1 - \rho^\chi)m_R + \rho^\chi m_R$. Solving (41) for $\hat{\boldsymbol{\delta}}$ and using $\|\hat{\boldsymbol{\delta}}\| = 1$ we arrive at the following condition for loss of uniqueness

$$\left|\frac{a + \xi^2 a'}{c}\right| = \| - \mathscr{L}^{-1} : \mathbf{N}\| \tag{42}$$

Since a and $\xi^2 a'$ are positive the condition (42) takes the form

$$\| - \mathscr{L}^{-1} : \mathbf{N}\| \geqslant \left|\frac{a}{c}\right| = \left|\frac{m_R - \rho^\chi m_R + \rho^\chi}{\rho_\chi}\right| \tag{43}$$

With limitation $m_R > 0$ and $0 < \rho < 1$ (43) may be fulfilled only if $\|\mathscr{L}^{-1} : \mathbf{N}\| > 1$ that is, in the stress range where the hypoplastic model itself yields non-unique solutions, see Reference 3. Thus, the uniqueness of (34) has been proved provided that equation (1) is unique.

APPENDIX C

We demonstrate now (after Malvern[40]) that the co-rotational rate $\hat{\dot{\boldsymbol{\delta}}}$ is objective. The constitutive law is written tensorially and involves gradients of velocity only so it is immune against any change of the co-ordinate system. This invariance of the formulation with respect to the rotated co-ordinate system can be written as $\dot{\mathbf{T}}(\mathbf{Q}\cdot\mathbf{T}\cdot\mathbf{Q}, \mathbf{Q}\cdot\boldsymbol{\delta}\cdot\mathbf{Q}, \mathbf{Q}\cdot\mathbf{D}\cdot\mathbf{Q}, e) = \mathbf{Q}\cdot\dot{\mathbf{T}}(\mathbf{T}, \boldsymbol{\delta}, \mathbf{D}, e)\cdot\mathbf{Q}$ where $\mathbf{Q}(=\text{constant})$ is an orthogonal matrix of rotation. A shift of time axis does not matter since time does not appear explicitly in the equations. A shift of the origin of the co-ordinate system does not matter either since the location in space does not enter the constitutive relation.

The requirement of frame indifference goes further than that. According to this requirement any inertial observer (no change of acceleration relative to the fixed stars) should measure the same values involved in the constitutive equations. It means that the matrix of rotation $\mathbf{Q}(t)$ and drift of the origin $\mathbf{c}(t)$ of space co-ordinates may be a function of time (but not of space). The co-rotational stress rate and the rate of deformation are frame indifferent too, see Reference 40. The co-rotational rate of $\boldsymbol{\delta}$ can be formulated analogously as the one of stress. Consider an alternative observer rotated with respect to the main one by $\mathbf{Q}(t)$. It measures the rate of $\boldsymbol{\delta}$ as

$$\dot{\boldsymbol{\delta}}^* = \dot{\mathbf{Q}}\cdot\boldsymbol{\delta}\mathbf{Q}^T + \mathbf{Q}\cdot\dot{\boldsymbol{\delta}}\mathbf{Q}^T + \mathbf{Q}\cdot\boldsymbol{\delta}\dot{\mathbf{Q}}^T \tag{44}$$

Since (see Reference 40) $\dot{\mathbf{Q}} = \mathbf{W}^*\cdot\mathbf{Q} - \mathbf{Q}\cdot\mathbf{W}$ and $\dot{\mathbf{Q}}^T = -\mathbf{Q}^T\cdot\mathbf{W}^* + \mathbf{W}\cdot\mathbf{Q}^T$ we obtain $\hat{\dot{\boldsymbol{\delta}}} = \dot{\boldsymbol{\delta}} - \mathbf{W}\cdot\boldsymbol{\delta} + \boldsymbol{\delta}\cdot\mathbf{W}$ as an objective co-rotational rate of $\boldsymbol{\delta}$.

REFERENCES

1. D. Kolymbas, 'An outline of hypoplasticity,' *Archive of Applied Mechanics*, **61**, 143–151 (1991).
2. D. Kolymbas and W. Wu, 'Introduction to hypoplasticity,' in *Modern Approaches to Plasticity*, ed. D. Kolymbas, Elsevier, pp. 213–223, 1993.
3. A. Niemunis, 'Hypoplasticity vs. elastoplasticity, selected topics,' in *Modern Approaches to Plasticity*, ed. D. Kolymbas, Elsevier, pp. 277–307, 1993.
4. W. Wu and E. Bauer, 'A simple hypoplastic constitutive model for sand,' *Int. j. numer. anal. methods geomech.*, **18**, 833–862 (1994).
5. D. Kolymbas, I. Herle and P. von Wolffersdorff, 'Hypoplastic constitutive equation with internal variables,' *Int. j. numer. anal. methods geomech.*, **19**, 415–436 (1995).
6. G. Gudehus, 'A comprehensive constitutive equation for granular materials,' *Soils and Foundations*, **36** (1), 1–12 (1996).
7. E. Bauer, 'Calibration of a comprehensive hypoplastic model for granular materials,' *Soils and Foundations*, **36** (1), 13–26 (1996).
8. P.-A. von Wolffersdorff, 'A hypoplastic relation for granular materials with a predefined limit state surface,' *Mech. cohesive-frictional mater.*, **1**, 251–271 (1996).
9. F. Darve, 'Incrementally nonlinear constitutive relationships', in *Geomaterials. Constitutive Equations and Modelling*, ed. F. Darve, pp. 213–237, 1990.
10. E. Bauer and W. Wu, 'A hypoplastic model for granular soils under cyclic loading,' in *Modern Approaches to Plasticity*, ed. D. Kolymbas, Elsevier, pp. 247–258, 1993.
11. R. J. Jardine, M. J. Symes and J. B. Burland, 'The measurement of soil stiffness in the triaxial apparatus,' *Géotechnique*, **34**, 323–340 (1984).
12. D. C. F. Lo Presti, 'Measurement of shear deformation of geomaterials in the laboratory,' *Int. Symp. on Pre-failure Deformation Characteristics of Geomaterials*, Hokkaido, pp. 1067–1088, 1994.
13. J. H. Atkinson, D. Richardson and S. Stallebrass, 'Effect of recent stress history on the stiffness of overconsolidated soil,' *Géotechnique*, **40** (4), 531–540 (1990).
14. G. Gudehus, M. Goldsheider and H. Winter, 'Mechanical properties of sand and clay and numerical integration methods: some sources of errors and bounds of accuracy,' in *Finite Elements in Geomechanics*, ed. G. Gudehus, Wiley, 1977.
15. J. N. Israelachvili, *Intermolecular and surface forces*, Academic Press, 1992.
16. T. A. Hueckel, 'Water–mineral interaction in hygromechanics of clays exposed to environmental loads: a mixture-theory approach,' *Can Geotech. J.*, **29**, 1071–1086 (1992).
17. G. Gudehus, 'Constitutive relations for granulate-liquid mixtures with a pectic constituent,' *Mechanics of Materials*, **22**, 93–103 (1996).
18. A. Casagrande, 'Characteristics of cohesionless soils affecting the stability of earth fills,' *J. Boston Soc. Civil Eng.*, in *Contributions to Soil Mech.*, 1925–1940 (1936).
19. C. Truesdell and W. Noll, 'The nonlinear field theories of mechanics,' in *Handbuch der Physik III/c*, Springer-Verlag, 1965.
20. W. Wu and A. Niemunis, 'Failure criterion, flow rule and dissipation function derived from hypoplasticity,' *Mech. cohesive-frictional mater.*, **1**, 145–163 (1996).
21. I. Herle, 'Granulometric properties and hypoplasticity of non-cohesive granular materials', Ph.D. Thesis, under preparation, 1996.
22. Z. P. Bazant and C.-L. Shieh, 'Hysteretic fracturing endochronic theory for concrete.' *J. Eng. Mech. Div., EM5*, **106**, 921–949 (1980).
23. Z. Mróz, 'On hypoelasticity and plasticity approaches to constitutive modelling of inelastic behaviour of soils,' *Int. j. numer. anal. methods geomech.*, **4**, 45–55 (1980).
24. R. S. Rivlin, 'Some comments on the endochronic theory of plasticity,' *Int. J. Solids Structures*, **17**, 231–248 (1981).
25. I. S. Sandler, 'On the uniqueness and stability of endochronic theories of material behaviour', *J. Applied Mech.*, **45**, 263–266 (1978).
26. S. A. Stallebrass, 'Modelling the effect of recent stress history on the deformation of overconsolidated soils,' Ph.D. Thesis, City University, 1990.
27. B. Simpson, 'Retaining structures: displacement and design,' *Géotechnique*, **42** (4), 541–576 (1992).
28. E. Guyon and J.-P. Troadec, *Du Sac de Billes au Tas de Sable*, Editions Odile Jacob, 1994.
29. U. Landman, W. D. Luedtke, N. A. Burnham and R. J. Colton, 'Atomistic mechanisms and dynamics of adhesion, nanoindentation, and fracture,' *Science*, **248**, 454–461 (1990).
30. H. Yoshizawa, Y.-L. Chen and J. Israelachvili, 'Fundamental mechanisms of interfacial friction. 1. Relation between adhesion and friction,' *J. Physical Chemistry*, **97** (16), 4128–4140 (1993).
31. K. von Terzaghi, *Erdbaumechanik auf Bodenphysikalischer Grundlage*, Franz Deuticke, Leipzig, Wien, 1925.
32. W. Wu and D. Kolymbas, 'Numerical testing of the stability criterion for hypoplastic constitutive equations,' *Mechanics of Materials*, **9**, 245–253 (1990).
33. P. Vermeer, 'A five constant model unifying well established concepts,' *Proc. Int. Work. on Constit. Relat. for Soils*, Grenoble, pp. 175–198, 1982.
34. M. Topolnicki, G. Gudenhus and B. K. Mazurkiewicz, 'Observed stress–strain behaviour of remoulded saturated clay under plane strain conditions,' *Géotechnique*, **40** (2), 155–187 (1990).
35. P.-A. Wolffersdorff, 'Probebelastung zur Baugrundtagung 1990: Bodendaten,' *Geotechnik*, **1**, 44–46 (1990).

36. S. Toki, F. Tatsuoki, S. Miura, Y. Yoshimi, S. Yasuda and Y. Makihara, 'Cyclic undrained triaxial strength of sand by a cooperative test program,' *Soils and Foundations*, **26** (3), 117–128 (1986).
37. D. Kolymbas, 'Computer-aided design of constitutive laws,' *Int. j. numer. anal. methods geomech.*, **15**, 593–604 (1991).
38. W. Wu, E. Bauer and D. Kolymbas, 'Hypoplastic constitutive model with critical state for granular materials,' *Mechanics of Materials*, **23**, 45–69 (1996).
39. J. Ohde, 'Zur theorie der druckverteilung im baugrund,' *Bauingenieur*, **20**, 451–459 (1939).
40. L. D. Malvern, *Introduction to the Mechanics of a Continuous Medium*, Prentice Hall, 1969.
41. M. Jamiolkowski, R. Lacellotta, D. C. F. Lo Presi and O. Pallara, 'Stiffness of Toyoura sand at small and intermediate strain,' *Proc. XII ICSMFE*, New Delhi, pp. 169–172, 1994.

